Institute of Space and Aeronautical Science, University of Tokyo
Report No. 593, March 1981

Experimental and Analytical Study of CO_2/N_2 Mixing Gasdynamic Laser

By

Kazuo MAENO*, Katsushi FUNABIKI and Hakuro OGUCHI

Abstract: This paper gives the results of experimental investigation of CO_2/N_2 mixing gasdynamic laser by means of synchronizing operation of two nondiaphragm shock tubes, together with the quasi-one-dimensional analysis based on instantaneous mixing assumption. By the satisfactory synchronization of shock reflections, separately heated CO_2 and N_2 are mixed to accomplish the population inversion, using two-dimensional or conical screen nozzle. The small signal gain coefficient measured was compared with the estimate by the analysis. Also the measurement of lasing power and the observation of flow field by Schlieren method were supplementarily conducted. As the results, the gain coefficient measured can be simulated qualitatively by the estimate, except for higher stagnation temperature rang of CO_2 (+He) above 1500°K. As for a fixed nozzle configuration, the existence of optimum stagnation conditions for CO_2/N_2 mixing GDL is clarified. The superiority of supersonic downstream injection by screen nozzle is also ascertained.

1. INTRODUCTION

By investigations of CO_2 gasdynamic laser (GDL) so far worked out, limited performance potential of conventional premixed CO_2 GDL has been noticed. This limitation of power is likely to be due to the dissociation of CO_2, collisional loss of vibrational energy in forward portion of nozzle and viscous losses by small throat size under severe operational conditions [*1*, *2*]. To circumvent these deficits, several advanced types of CO_2 GDL are investigated [*3*]. Among them, CO_2/N_2 mixing GDL shows the most favorable potential with utilizing separately pumped N_2 by thermal means. Several researches [*4–7*] have been performed to clarify an improved characteristics of this concept. Comprehensive reviews should be referred to Refs. [*2*] and [*8*].

As for the mixing of CO_2 with catalyst into a donor gas N_2, various methods have been noticed and contrived. Taran et al. [*4*, *9*] obtained the results by central throat injection scheme, using arc heater to supply supersonic N_2 flow. The concept of side wall or slotted tube injection was investigated by Croshko et al. [*5*, *10*, *11*] using shock tube. These techniques are characterized as throat or near-throat injection of the sonic flow of CO_2 (with catalyst He or H_2O) with room temperature. Though this concept has the merits of reducing the mixing loss due to velocity diffrence between N_2 flow and injected CO_2, and of minimizing the disturbances from pressure difference,

* Tokyo Metropolitan College of Aeronautical Engineering.

it must suffer from the conflict of high freezing efficiency and favorable medium homogeneousness.

Schall et al. [7] compared experimentally three mixing schemes, which were the injection from central throat, side wall injection, and the mixing by screen nozzle with sonic injection of unheated CO_2/He. From their results, it was remarked that screen nozzle was superior to other schemes. This scheme, however, involves increased mixing loss caused by velocity discrepancy with sonic injection of CO_2, despite the efficient vibrational freezing of donor gas N_2.

On the other hand, Cassady et al. [6, 8] investigated the downstream mixing by screen nozzle with supersonic injection of CO_2/H_2O from electrically preheated oven, and obtained favorable performance along with the good optical quality of mixed flow by avoiding the mixing loss and disturbances. This concept, however, introduces an additional preheating of injecting flow and also involves noequilibrium effects in CO_2 flow.

Throughout the progress of these investigations, the shock tube has played an important part of experiment, because of the feasibility to cover a wide range of flow conditions. In this paper we aim to clarify the noequilibrium effects of CO_2 flow and some of fundamental characteristics of CO_2/N_2 mixing GDL by synchronizing operation of two shock tubes over a wide range of stagnation conditions of the component. Also a simple numerical analysis based on instantaneous mixing assumption and three mode model of vibrational state for CO_2/N_2/He system is presented.

2. Experimental Apparatus

2.1 *Shock tubes*

In this experiment, a couple of shock tubes were employed so as to produce the

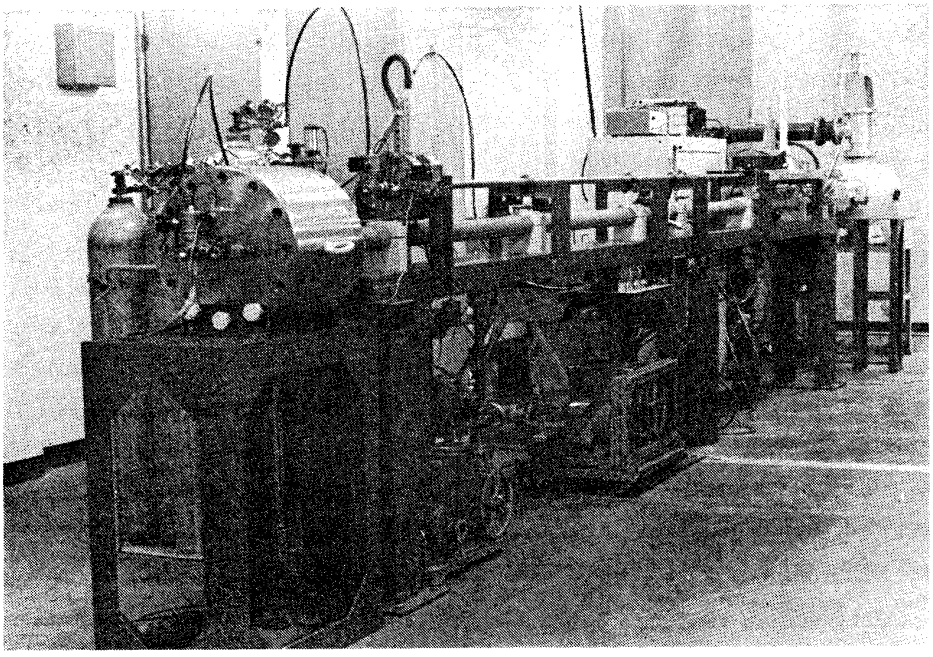

Fig. 1. Experimental apparatus.

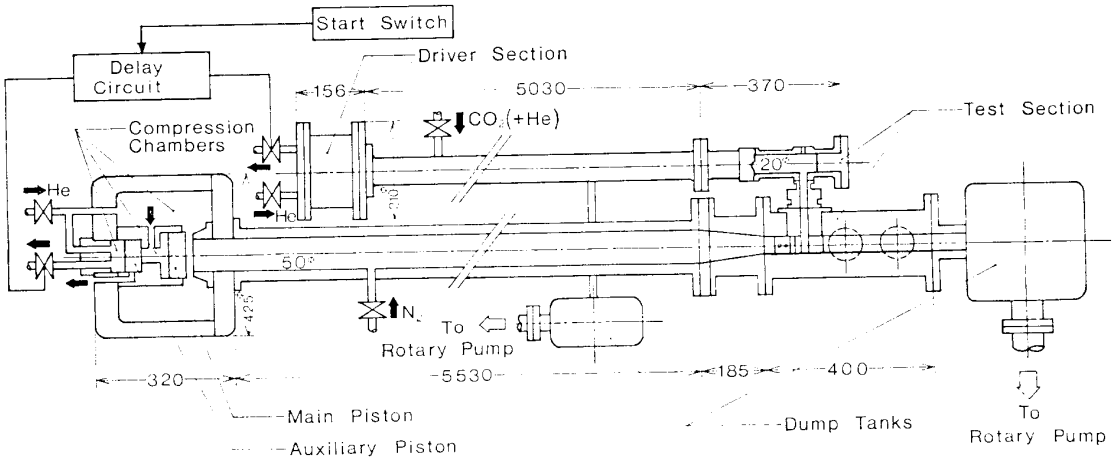

FIG. 2. Schematic diagram of two-shock-tube apparatus.

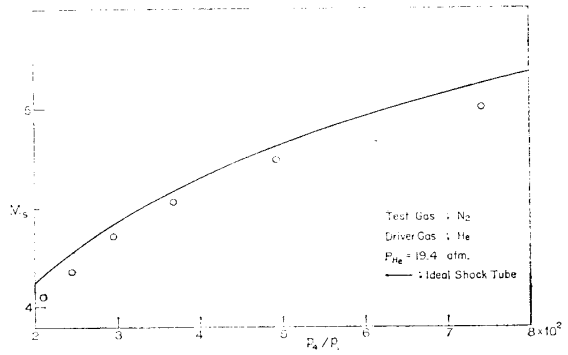

FIG. 3. Operational characteristics of N_2 shock tube.

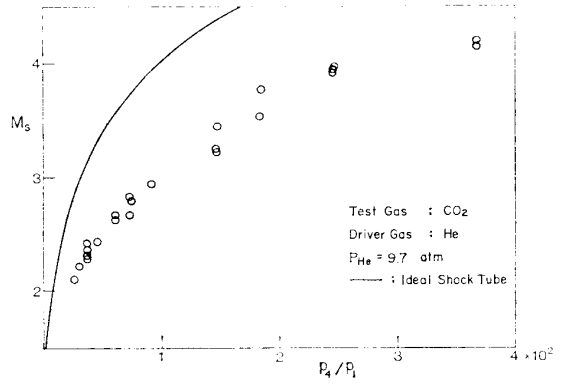

FIG. 4. Operational characteristics of CO_2 shock tube.

separate stagnation conditions for CO_2 (or + He) and N_2. Each shock tube has a same driving mechanism; that is, the tube is deviced to be driven by a fast actuating free-piston valve controlled by a small auxiliary valve [*12*, *13*]. This type of shock tube is much favorable compared with a conventional shock tube in reproducibility, operation, and protection from any contaminations.

The whole picture of the shock tubes and the schematic are shown in Figs. 1 and 2. Here we briefly note the driving mechanism as well as the performance of this

type of shock tube, whose details have already been reported in the previous paper [12]. The high pressure gas (He) is supplied from the inlet into the high pressure plenum as well as auxiliary piston cylinder. The auxiliary piston is pushed forward and intercepts the main piston cylinder from the discharge tube. Then, with the pressure rise at the main piston cylinder, the main piston is pushed forward to intercept the high pressure plenum from the evacuation tube (driven tube). This is the set up of the valve closing. As for the openning, it can be made by openning the small magnetic valve, equipped outside of the plenum. With sudden release of high pressure gas behind, the auxiliary piston is moved back. Then, the gas behind the main piston is discharged into atmosphere and moved back. Consequently, the plenum is discharged into the driven tube. The process mentioned above can easily be repeated by on-off control of a small magnetic valve.

Regarding the performance, the shock Mach numbers measured are plotted versus the pressure ratio p_4/p_1 of the driver to the driven section in Fig. 3 for the main shock

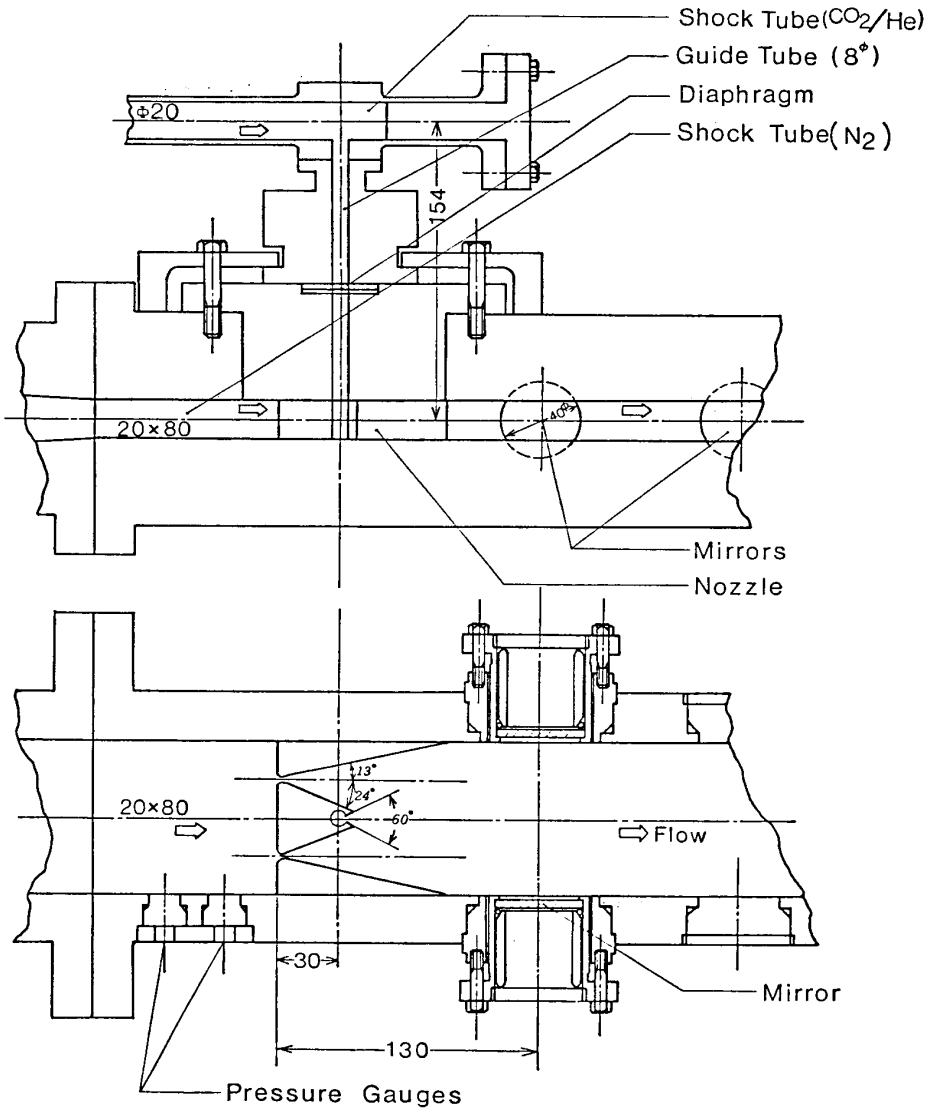

FIG. 5. Test section for CO_2/N_2 mixing GDL.

tube using N_2 as test gas and He as driver gas. In the figure, the relation from the ideal shock tube theory is also plotted. The similar results are shown in Fig. 4 for the smaller shock tube using $CO_2(+He)$ as test gas and He as driver gas.

2.2 *Test section and nozzles*

The rectangular section of 80×20 mm is jointed through a distant adaptor with the circular section 50 mm in in. diam.. The nozzle is mounted at most forward portion of the test section. The end portion of CO_2 tube is connected with the nozzle through a guide tube of 8 mm in in. diam., and primarily separated from the nozzle and the N_2 tube by a sheet of polyethylene thin enough to be broken at the arrival of shock wave in the CO_2-tube. The schematic of the test section equipped with the two-dimensional nozzle is shown in Fig. 5. As can be seen from this figure, the test gas CO_2, heated and compressed by a reflected shock wave at the end of the CO_2-tube, is expanded through the nozzle and mixed with the test gas N_2 expanded through the main nozzle. The test gas N_2 is also heated by the reflected shock at the forward face of the main nozzle. Apparently, the production of mixing flow requires a precise synchronization of both the N_2- and CO_2-tubes. In this experiment, three types of two-dimensional nozzles and a conical screen nozzle were employed (Fig. 6). As shown in Fig. 6, the injection port of CO_2 is inserted between a couple of 2-D nozzles for N_2. The type of CO_2 injection was altered by using three different types of the injection port.

The velocity of incident shock was measured by a couple of piezoelectric pressure gauge (Kistler CO. Ltd), and also the pressure history of both incident and reflected shock waves was recorded for each tube.

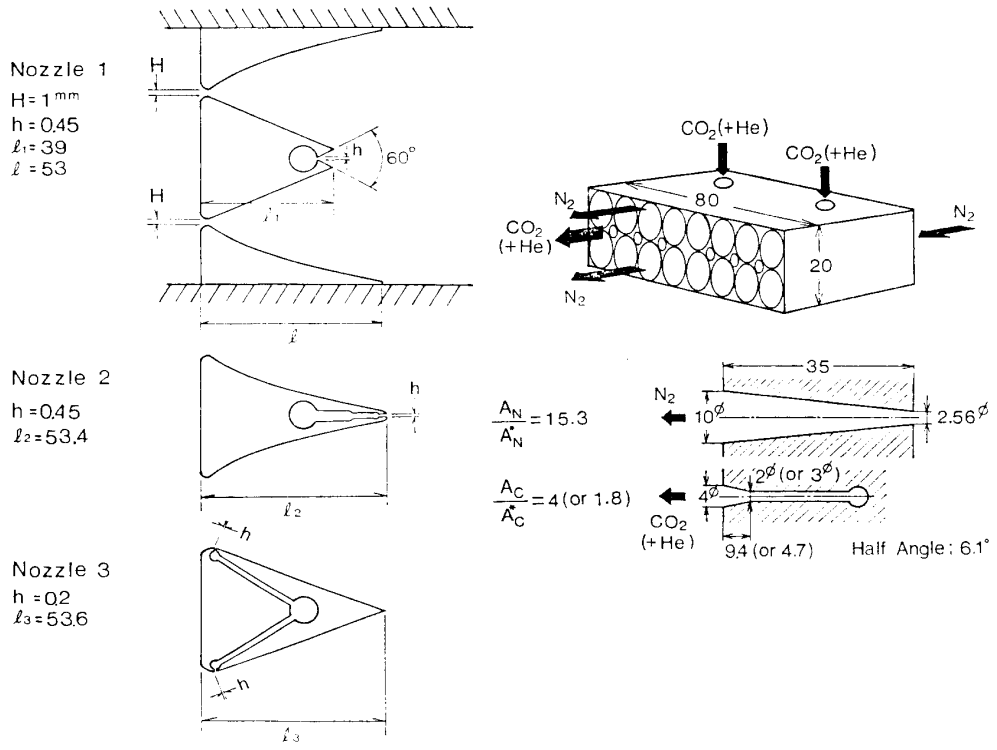

FIG. 6. Nozzles used for CO_2/N_2 mixing GDL.

2.3 *Laser cavity and infrared detector*

Laser power of 10.6 μm was derived by means of a stable resonator. This resonator consists of Ge concave total reflector with 10 m radius of curvature and Ge plane partial reflector with 1.5% transmittance. These mirrors were adjustable and mounted in the test section windows with small recess of about 3 mm from the nozzle walls. The threshold gain G_c for optical amplification is given with neglection of a coupling loss as follows:

$$G_c=\frac{1}{L_c}\left(\frac{1-r_1}{1+r_1}+\frac{1-r_2}{1+r_2}\right)$$

where

$$r_n=1-d_n-t_n \qquad (n=1,2)$$

L_c is the cavity path transverse to the flow, d_n and t_n denote, respectively, the optical loss and the transmissivity of each mirror. For our resonator G_c was equal to 0.105 (1/m).

In the measurement of the lasing power, a dewar-type Hg-Cd-Te ptotoconductive infrared detector cooled by LN_2 was employed. The detector was calibrated by using a CO_2 CW laser and conventional power meter (Coherent Radiation Labs. Model 210).

2.4 *Measurement of small signal gain coefficient*

For the measurement of small signal gain coefficient G, CW CO_2 probe laser and Hg-Cd-Te detector were also used along with Ge windows of 98% transmissivity and Ge partial reflector with 15% transmissivity. As shown in Fig. 7, the diagnostic beam from CW CO_2 laser is attenuated by a diffusive Al reflector, and then passed through the windows of test section. The intensity of the beam is furthermore diminished to be adequate for the detector measurement by partial reflector and polyester sheets. An electro-magnetic shutter for protection of the detector from CW laser is opened by a trigger signal. Then, the beam intensity is recorded by the digital transient recorder (Data Lab. Model DL 905).

The gain coefficient G is given by

$$G=\frac{1}{L_c}\ln\left(\frac{I_0+\Delta I}{I_0}\right)$$

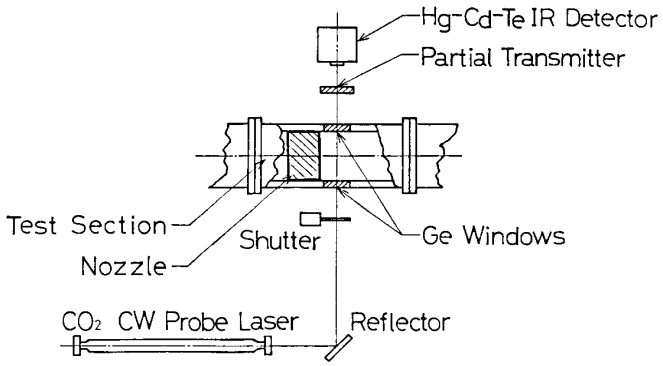

Fig. 7. Block diagram of gain measurement.

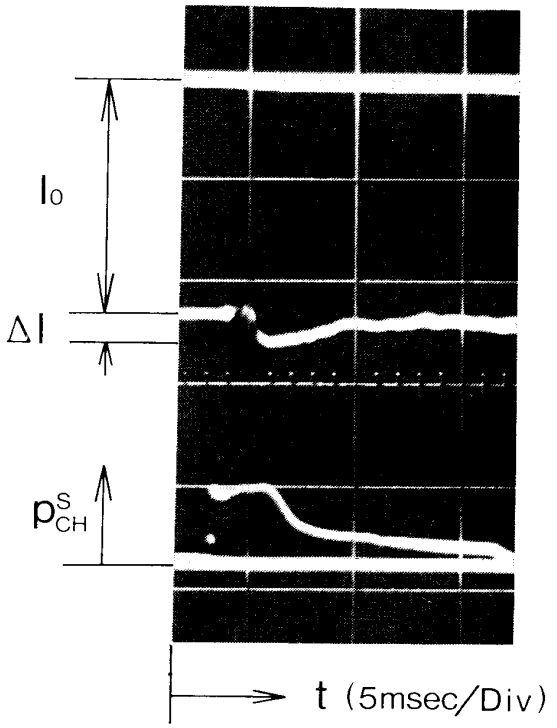

FIG. 8. Probe laser signal for gain measurement together with pressure signal of CO_2 tube.

where I_0 is the initial intensity, ΔI the increment and the cavity path L_c may be taken to be equal to the length of active medium. The spot diameter of probe laser beam was about 4 mm, and the attenuated intenisty of beam was kept from 0.1 to 0.2 w/cm^2 weak enrough to avoid interference with the flow [1]. Care was taken to keep off the mechanical vibration of optical system.

Typical gain signal observed is shown in Fig. 8 together with the pressure history at the CO_2-tube end. Synchronization of the shock reflection of CO_2-tube end with that of the N_2-tube is monitored by the brightness control of the synchroscope sweep of the pressure record.

2.5 *Experimental conditions*

The small signal gain coefficients were measured with varying nozzle stagnation conditions. Also the lasing power were measured for cases of two-dimensional nozzle. For comparison the measurement was made for premixed CO_2 GDL. The stagnation conditions which were covered in this experiment were as follows:

$$2\ \text{atm} < p_c^s < 6\ \text{atm}, \qquad 500°\text{K} < T_c^s < 2400°\text{K}$$
$$2\ \text{atm} < p_{CH}^s < 5\ \text{atm}, \qquad 700°\text{K} < T_{CH}^s < 2300°\text{K}$$
$$5\ \text{atm} < p_N^s < 10\ \text{atm}, \qquad 2000°\text{K} < T_N^s < 3500°\text{K}$$

where p^s and T^s denote the pressure and temperature of stagnation, and subscripts C, N and CH indicate CO_2, N_2 and the mixture of CO_2/He, respectively. These conditions were evaluated using the ideal shock relations with the measured velocity of incident shock wave. We note here that the minicomputer HITAC-10 II was used

to support on/off line processings of experimental data and also that Schlieren photographs were taken to observe the flow behavior.

3. Numerical Estimate of Laser Performance

A simple analysis for CO_2/N_2 mixing GDL was performed under the assumptions of three-mode model for vibrational relaxation, instantaneous mixing, and inviscid, quasi one-dimensional flow. In comparison with the previous analyses [*4*, *14*], this estimate has a great simple aspect and also feasible applicability to complicated flow structures. Soloukhin et al [*2*, *10*] performed a similar analysis and applied to their experiment. In distinction from their analysis for sonic injection of room temperature CO_2, our estimate takes into account nonequilibrium processes in both N_2 and CO_2 flows.

3.1 *Formulation*

The flow is assumed to be in translational and rotational equilibrium. The equations for steady, inviscid, quasi one-dimensional, vibrational nonequilibrium nozzle flow of $CO_2/N_2/He$ are given as follows

$$\frac{d}{dx}(\rho u A)=0$$

$$\rho u\frac{du}{dx}+\frac{dp}{dx}=0$$

$$\frac{d}{dx}\left(C_pT+e^v+\frac{u^2}{2}\right)=0$$

$$p=R\rho T$$

where

$$C_p=\frac{\bar{R}}{M_m}\left\{\frac{7}{2}(\psi_C+\psi_N)+\frac{5}{2}\psi_H\right\}$$

and specific vibrational energy e^v is given as

$$e^v=C_C(e_1^v+2e_2^v+e_3^v)+C_Ne_N^v$$

Here $\bar{R}$ is the universal gas constant, ψ_i is the molar fraction of i-th component in the mixture, M_m is mean molecular weight, C_i the mass fraction of i-th component, the subscripts C, N and H indicate CO_2, N_2 and He respectively, e_j^v the j-th mode vibrational energy ($j=1, 2, 3, N$) in CO_2/N_2 system. The j-th mode vibrational energy e_j^v is

$$e_j^v=\frac{R_i\theta_j}{\exp(\theta_j/T_j)-1}\qquad(i=C, N)$$

where T_j denotes local equilibrium vibrational temperature of the j-th mode and the

vibrational characteristic temperature.

Several models of vibrational relaxation equations for CO_2/N_2 system have been proposed [*15–17*]. Under the assumptions of harmonic oscillator in vibration, of local thermal equilibrium (Trenor Equilibrium) within each mode, and of mutual equilibrium within ν_1 and ν_2 modes of CO_2 by Fermi Resonance, three-mode model of $CO_2/N_2/He$ system can be employed. The relaxation equations are derived from the general equation of CO_2 relaxation by Sato and Tsuchiya [*18*]; that is,

$$u\frac{de_{12}^v}{dx}=u\frac{d}{dx}(e_1^v+2e_2^v)$$

$$=\frac{2}{\tau}(e_2^{v(e)}-e_2)+e_2^{v(e)}\frac{2}{\tau_{3,12}}\cdot\frac{E}{\exp(-\theta_1/T)(\exp(\theta_3/T)-1)}$$

$$u\frac{de_3^v}{dx}=e_3^{v(e)}\left[-\frac{2}{\tau_{3,12}}\cdot\frac{E}{(1-\exp(-\theta_1/T))}+\frac{\psi_N}{\tau_{3,4}}\cdot\frac{E}{(1-\exp(-\theta_N/T))}\right]$$

$$u\frac{de_N^v}{dx}=-e_N^{v(e)}\cdot\frac{\psi_c}{\tau_{3,4}}\cdot\frac{F}{\exp(-\theta_N/T)(\exp(\theta_3/T)-1)}$$

where

$$E=\frac{e_3^v}{e_3^{v(e)}}\cdot\left\{1-\exp\left(-\frac{\theta_1}{T}\right)\cdot\left(1-\frac{e_1^v}{e_1^{v(e)}}\right)\right\}-\frac{e_1^v}{e_1^{v(e)}}\cdot\left\{1-\exp\left(-\frac{\theta_3}{T}\right)\cdot\left(1-\frac{e_3^v}{e_3^{v(e)}}\right)\right\}$$

$$F=\frac{e_N^v}{e_N^{v(e)}}\cdot\left\{1-\exp\left(-\frac{\theta_3}{T}\right)\cdot\left(1-\frac{e_3^v}{e_3^{v(e)}}\right)\right\}-\frac{e_3^v}{e_3^{v(e)}}\cdot\left\{1-\exp\left(-\frac{\theta_N}{T}\right)\cdot\left(1-\frac{e_N^v}{e_N^{v(e)}}\right)\right\}$$

$$e_j^{v(e)}=\frac{R_i\theta_j}{\exp(\theta_j/T)-1}\qquad(i=C,N)$$

Vibrational relaxation time τ denotes the time for translational-vibrational $(T-V)$ energy transfer process of ν_2 mode, and $\tau_{i,k}$ for intermolecular or intramolecular $V-V$ process between j-th mode and k-th mode. These are obtained from experimental data [*17, 20*] and by parallel resistance rule.

3.2 *Numerical procedure and mixing conditions*

For the numerical estimate, two nozzle flows of $CO_2(+He)$ and N_2 are dealt with separately. Using the assumption of vibrational equilibrium at upstream of the throat, the throat conditions can be calculated from the stagnation conditions. With these starting conditions, the flow from the throat toward downstream can be solved numerically by Runge-Kutta method.

Regarding the mixing of two nozzle flows, the followings are assumed.

(1) At the location of mixing, both flows are mixed instantaneously; that is, the mixing occurs at a plane across the flow (see Fig. 9).

(2) Vibrational temperatures $T_{12}(=T_1=T_2)$, T_3, T_N are not changed passing through the mixing plane.

(3) No strong disturbance such as shock wave is formed. A scheme of this type of mixing is illustrated in Fig. 9. According to the notation shown in Fig. 9, the con-

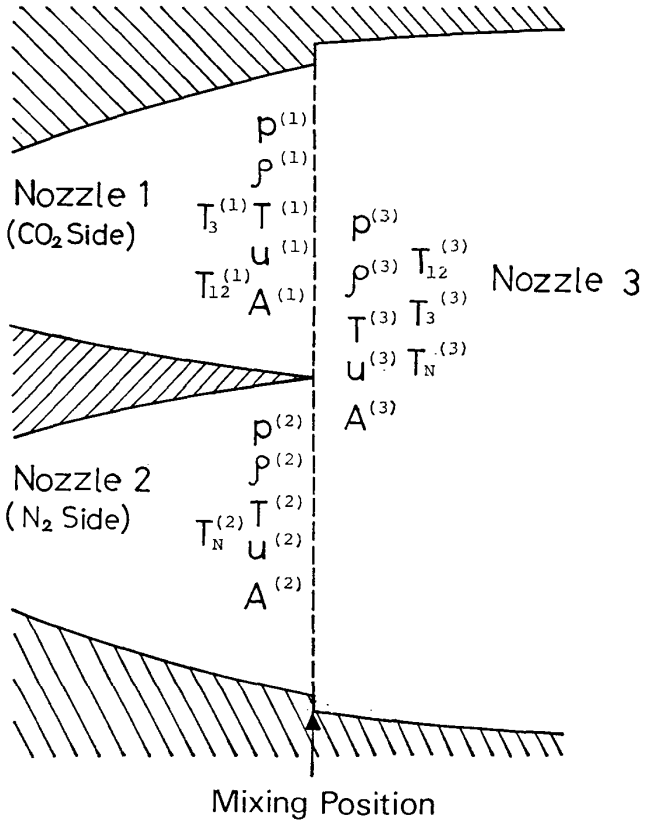

FIG. 9. Scheme for instantaneous mixing.

servation of species, total mass, total momentum and energy are written with the equation of state as follows:

$$C_i^{(1)}\rho^{(1)}u^{(1)}A^{(1)}+C_i^{(2)}\rho^{(2)}u^{(2)}A^{(2)}=C_i^{(3)}\rho^{(3)}u^{(3)}A^{(3)}\equiv D_i \qquad (i=C, N, H)$$

$$D=\sum_i D_i$$

$$P^{(1)}A^{(1)}+\rho^{(1)}u^{(1)2}A^{(1)}+p^{(2)}A^{(2)}+\rho^{(2)}u^{(2)2}A^{(2)}=p^{(3)}A^{(3)}+\rho^{(3)}u^{(3)2}A^{(3)}$$

$$\rho^{(1)}u^{(1)}A^{(1)}[C_p^{(1)}T^{(1)}+\tfrac{1}{2}u^{(1)2}]+\rho^{(2)}u^{(2)}A^{(2)}[C_p^{(2)}T^{(2)}+\tfrac{1}{2}u^{(2)2}]=\rho^{(3)}u^{(3)}A^{(3)}[C_p^{(3)}T^{(3)}+\tfrac{1}{2}u^{(3)2}]$$

$$p^{(3)}=R^{(3)}\rho^{(3)}T^{(3)}$$

In these equations, the vibrational energy terms are omitted as they are conserved automatically by the assumption (2).

These algebraic equations can be solved if the cross sectional area $A^{(3)}$ of the down-side of mixing location is given, and the conditions of the flow after mixing are obtained. Using these parameters for starting condition, the flow after mixing is solved numerically by the same procedure as that for the upetream side of the mixing location.

3.3 *Small signal gain coefficient*

Small signal gain coefficient G is given approximately by the relation [*1*]

$$G=\frac{\lambda^2}{4\pi\tau^* Z}(N_{C(001)}-N_{C(100)})\left(\frac{45.6}{T}\right)e^{-234/T}$$

where $P(20)$ rotational transition of the 10.6 μm band is supposed, and is the wavelength of CO_2 GDL equal to 10.6 μm, τ^* is the spontaneous radiative lifetime equal to 5.38 sec and Z represents the collision frequency

$$Z=\sum_i N_i \sigma_i V_{C-i}$$

N_i is the number density of i-th component gas, σ_i is the collision sectional area and V_{C-i} is the relative speed in collision between CO_2 and i-th component,

$$V_{C-i}=\left\{\frac{8\bar{R}T}{\pi}\left(\frac{M_C+M_i}{M_C M_i}\right)\right\}^{1/2}$$

The population inversion, which is a difference between number densities of upper laser energy level $CO_2(001)$ and lower level $CO_2(100)$ is obtained by

$$N_{C(001)}-N_{C(100)}=N_C\{\exp(-\theta_3/T_3)-\exp(-\theta_1/T_1)\}/Q_C^N$$

where Q_C^N is the vibrational partition function

$$Q_C^N=\left[1-\exp\left(-\frac{\theta_1}{T_1}\right)\right]^{-1}\left[1-\exp\left(\frac{\theta_2}{T_2}\right)\right]^{-2}\left[1-\exp\left(-\frac{\theta_3}{T_3}\right)\right]^{-1}$$

In numerical calculations, the spatial step Δx along the nozzle axis must satisfy a following criteria

$$\Delta x \leqq Bu(\tau_i)_{\min}$$

where u is the flow velocity, $(\tau_i)_{\min}$ is the least of relaxation times and a constant factor B is chosen to be from 0.01 to 0.05, empirically.

4. Results and Discussion

4.1 *Operation and synchronization of two shock tubes*

An example of data regarding the synchronization of the two shock tubes is shown in Fig. 10. Each run is designated by the experimental operation numbers, which are shown on the abscissa, while the ordinate represents the time measured from the start of trigger switch-on. Solid lines denote the durations of lasing observed by infrared detector. Pressure histories at both tube ends are also shown in Fig. 11. As can be seen from these data, the mismatch between two shock-tube runs was limited within about 400 μs.

4.2 *Laser power observed*

The power distribution over the partial transmitor of cavity was measured for CO_2/N_2 mixing GDL and also for the premixed GDL, in changing nozzle configurations (see Fig. 6). Without any optimization on power extraction from cavity mirrors, however the measurement was conducted.

Regarding the results for the power measurement, the followings are to be noticed.

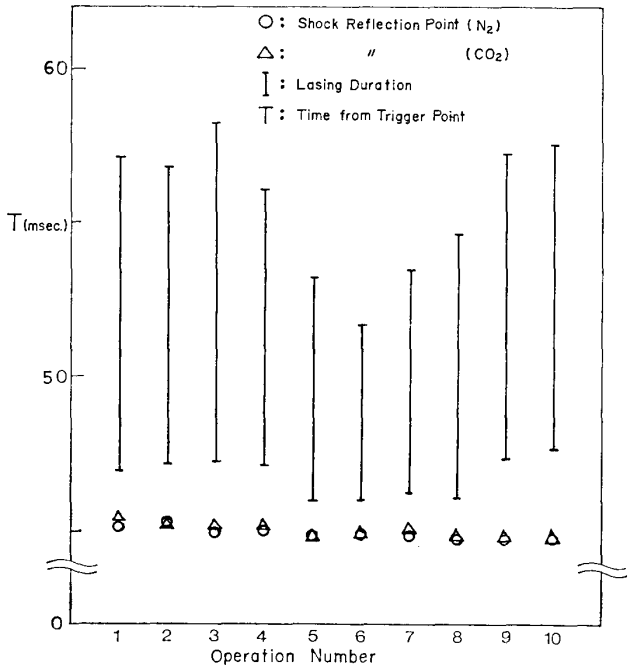

FIG. 10. Data for synchronizing operation of two shock tubes.

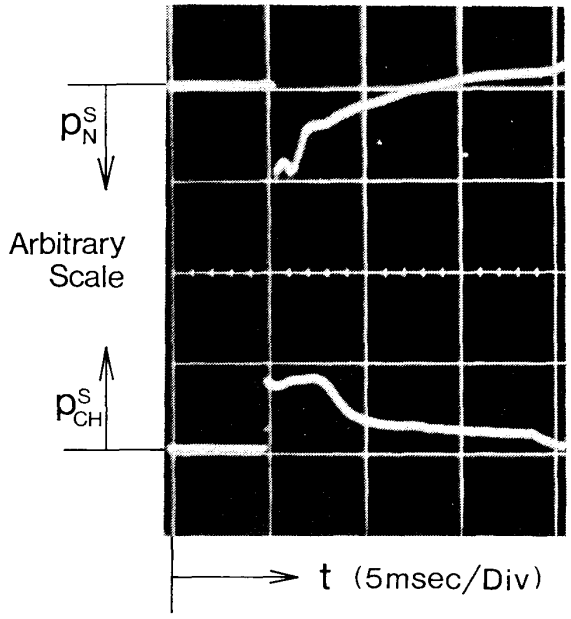

FIG. 11. Pressure histories at both tube ends.

1) Fast time variation with cycles of the order of microseconds and many high spikes of the power signal were observed. 2) The total powers of 10—30 w were extracted from the laser cavity. Especially, for the downstream mixing GDL using conical screen nozzle, comparatively higher power was observed even for the mixing of N_2 with pure CO_2, while no power was extracted in the premixed conventional GDL without catalyst. 3) The dependence of the power extracted at the cavity center on the stagnation condition was also measured for a fixed geometry of nozzle. Figures

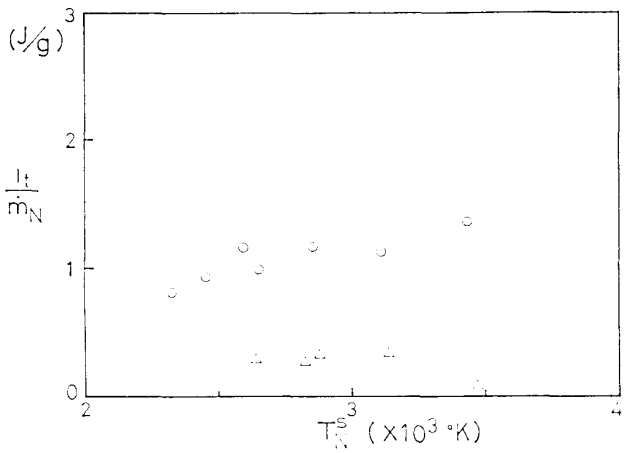

FIG. 12. Dependence of specific power $I_t/\dot{m}_N$ on N_2 stagnation temperature $T_N{}^S$.
○: $p_C{}^S$=6.5 atm, $T_C{}^S$=700° K
△: $p_C{}^S$:=4.2 atm, $T_C{}^S$=1600° K

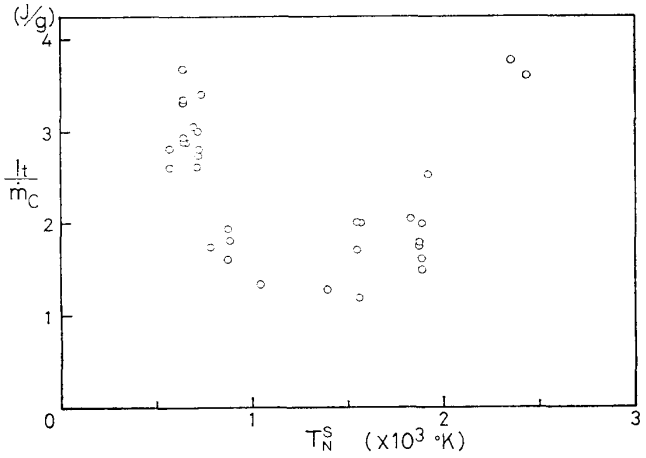

FIG. 13. Dependence of specific power $I_t/\dot{m}_C$ on CO_2 stagnation temperature $T_C{}^S$.
($p_N{}^S$=9 atm, $T_N{}^S$=2700° K)

12 and 13 show the results of the experiment for pure CO_2 mixing GDL using Nozzle I (see Fig. 6). Figure 12 represents the relation between the stagnation temperature T_N^s of N_2 and the total power I_t divided by the mass flux m_N of N_2 for a fixed condition of CO_2 reservoir. On the other hand, Fig. 13 shows the relation between T_C^s of CO_2 and I_t divided by CO_2 mass flux m_c for a fixed stagnation condition of N_2. In contrast to weak dependence of I_t/m_N on T_N^s, a strong dependence of I_t/m_C on T_C^s can be seen from these figures.

4.3 *Results of numerical evaluation for* CO_2/N_2 *mixing GDL*

Based upon our simple numerical method, the flow behaviors and nonequilibrium vibrational processes were analyzed for specified nozzle configuration and stagnation conditions. In Fig. 14 the vibrational temperatures (T_N, T_{12}, T_3), the translational temperature T and the small signal gain coefficient G are plotted versus the distance

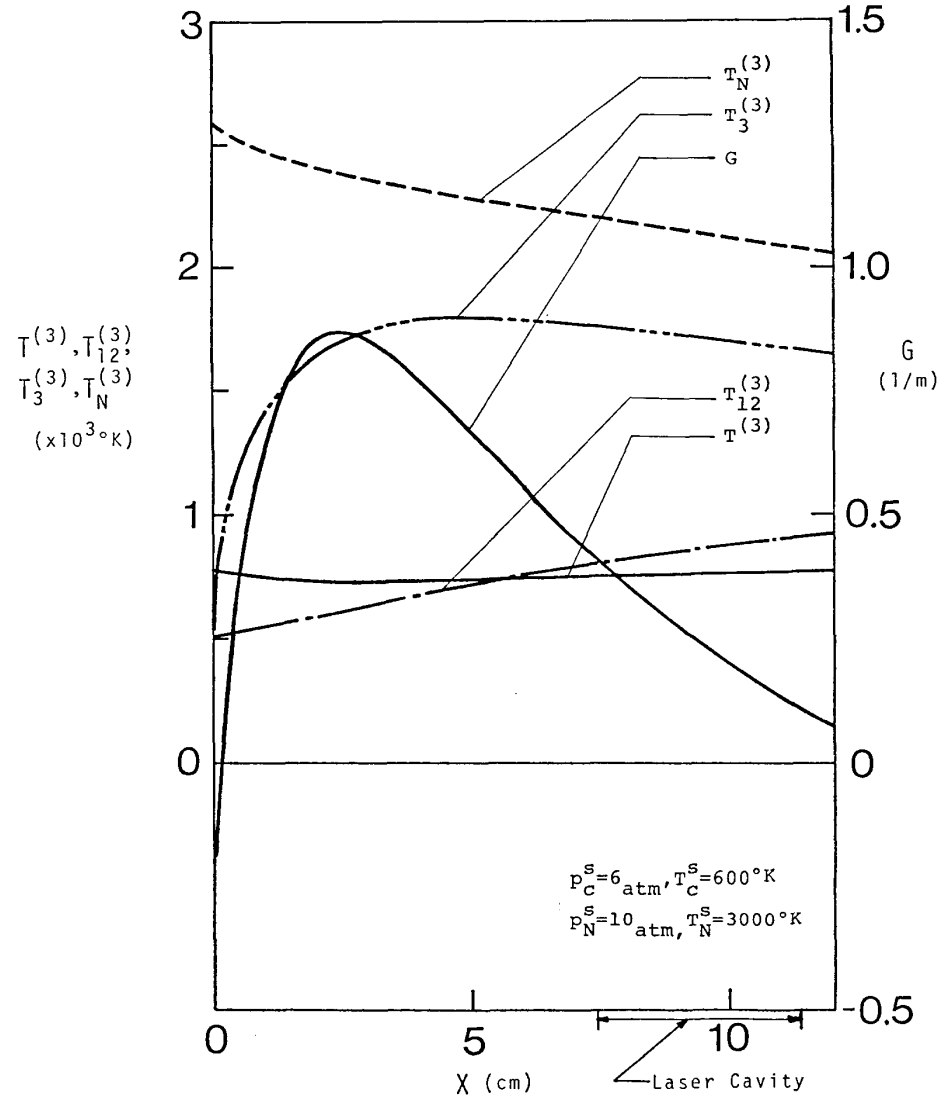

FIG. 14. Calculated distributions of temperatures and gain in the flow (for pure CO_2 mixing).

X from the beginning of mixing for the case of Nozzle I. The stagnation conditions p^s, T^s for CO_2 and N_2 nozzle flows are also given in the figure, along with the cavity location. As the results, the fast energy transfer from vibrational mode of N_2 to ν_3 mode of CO_2 causes rapid increase of $T_3^{(3)}$ and lead to successive steep increase of G, while the vibrational temperature $T_{12}^{(3)}$ of lower level mode of CO_2 increases much slowly toward downstream. The behavior of $T_{12}^{(3)}$ has a strong effect on gain such that G shows rapid decay following its peak. In the case when the stagnation temperature T_c^s is raised up to above 1000°K for the same nozzle configuration, $T_3^{(3)}$ becomes higher, but the increased level of $T_{12}^{(3)}$ is likely to impell the peak of G to a lower value.

In Fig. 15 the distributions of temperatures and G are represented for the case of the mixture 50 CO_2/50 He (in molar fraction) mixing with N_2 under the same conditions as shown in Fig. 14. The catalytic effect of He can obviously be seen and the

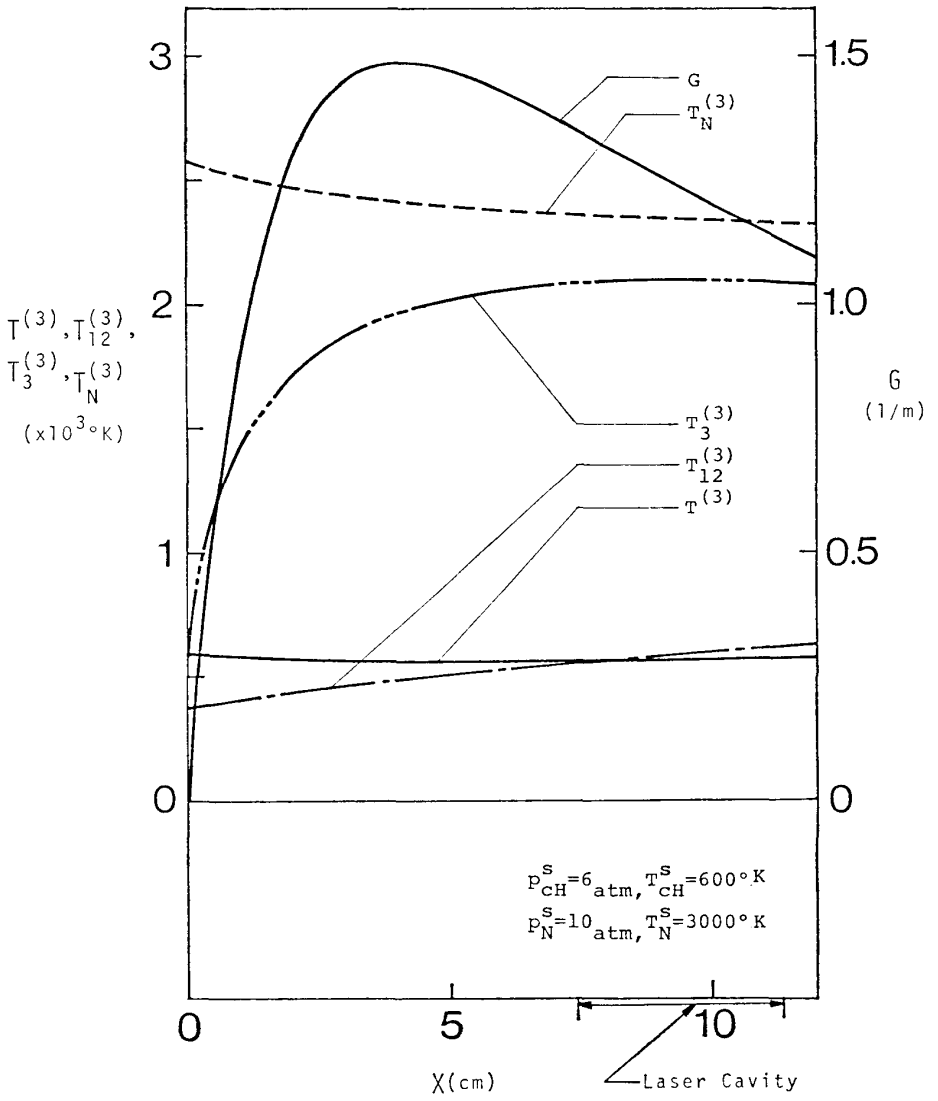

FIG. 15. Calculated distributions of temperatures of temperatures and gain in the flow (for 50% CO_2/50% He mixing).

distribution of G has a higher peak followed by more gradual decrease than that shown in Fig. 14. From the other numerical results, favorable characteristics of G is confirmed for the mixture of CO_2/He than for the mixture N_2/He.

The dependence of G on the nozzle configuration is demonstrated in Fig. 16, where three types of 2-D nozzles are compared. As for Nozzle 2 and 3 (see Fig. 6), CO_2/N_2 is mixed into N_2 flow under throat (sonic) conditions. The gain G at the cavity center is plotted versus the stagnation temperature T_{CH}^s. Molar fraction $\psi_C^{(3)}$of CO_2 is also plotted. As can be seen from the figure, Nozzle I, in which CO_2 is mixed with N_2 after expansion, seems to indicate most favorable characteristics for CO_2mixing GDL.

Next, the dependence of G on nozzle stagnation condition was examined. Figures 17 and 18 show variation of G at the cavity center, respectively, with stagnation pressure p_{CH}^s and with stagnation temperature T_N^s. Molar fraction of CO_2 is also denoted. From the results shown above, it must be remarked that optimum stagnation conditions exists for a specified nozzle configuration.

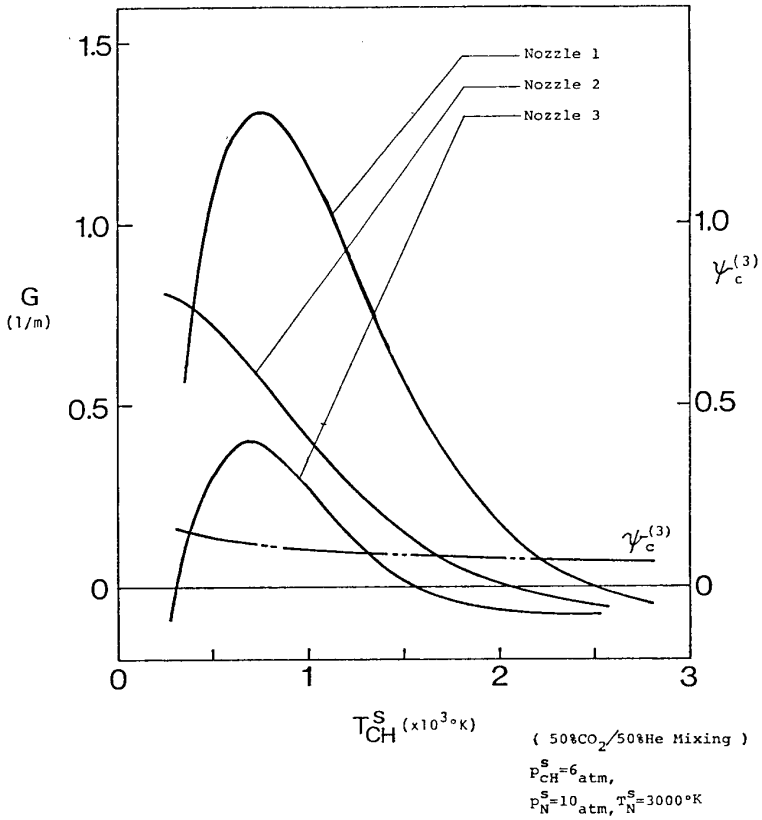

Fig. 16. Dependence of gain on stagnation temperature $T_{CH}{}^S$ for several mixing configurations.

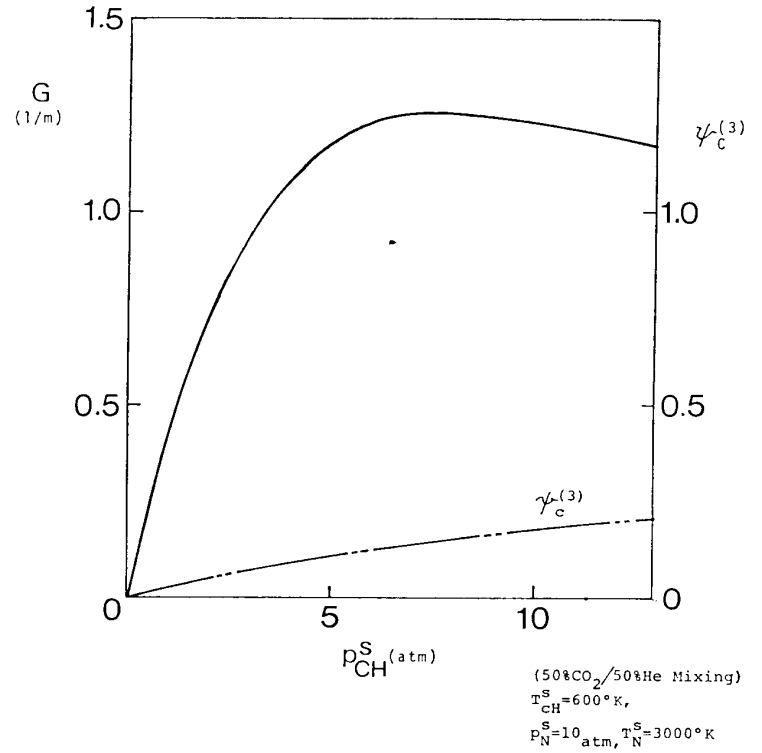

FIG. 17. Dependence of gain on stagnation pressure $p_{CH}{}^S$.

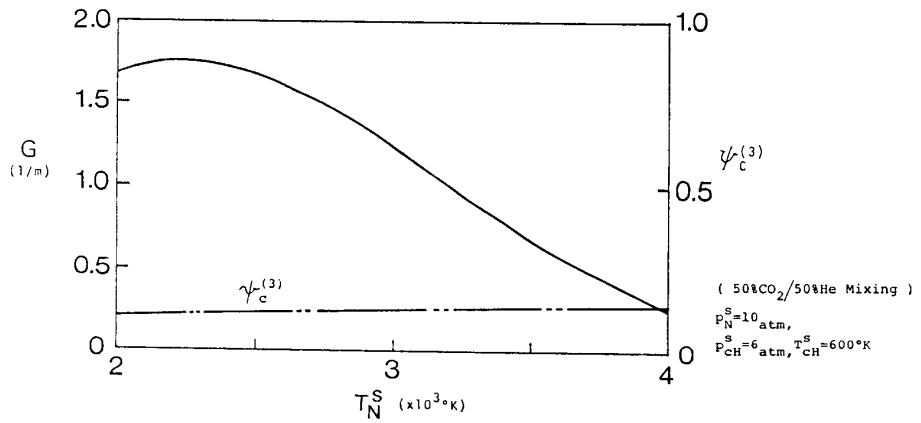

FIG. 18. Dependence of gain on stagnation temperature $T_N{}^S$.

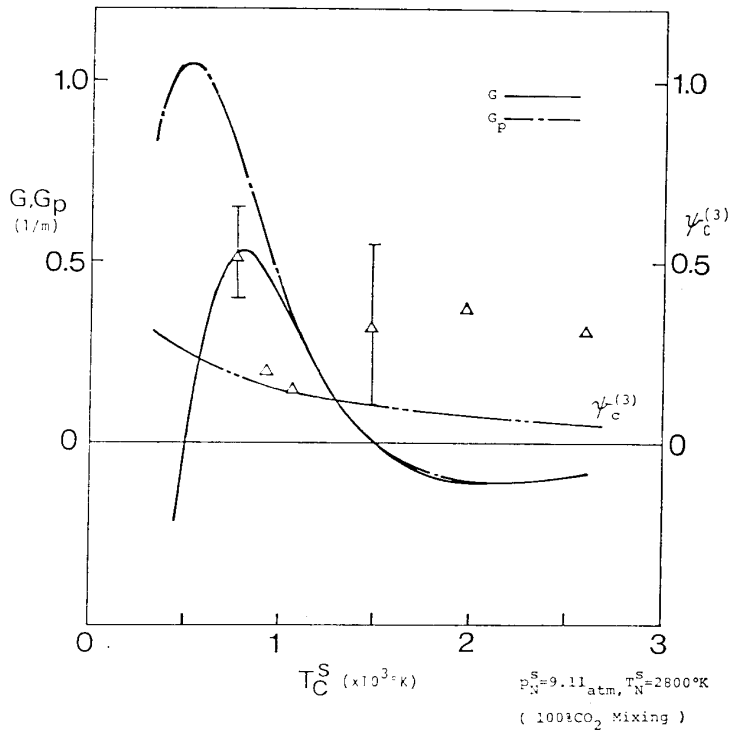

FIG. 19. Comparison of measured gain with estimated variation for $T_C{}^S$ (Nozzle 1).

4.4 *Comparison of experiment with numerical estimate*

In order to check the applicability of our numerical estimate to CO_2/N_2 mixing GDL, the numerical results were compared with the experiment. In the estimate the small signalgain G was evaluated for the rotational transition line of $P(20)$. In the measurement, however no selection of particular rotational line was made, because no significant difference was presumed to result in.

For the case of Nozzle I, the dependence of G at the cavity center on T_C^s is shown for a fixed N condition in Fig. 19. The molar fraction $\psi_C^{(3)}$of CO_2 is also plotted in the same figure. In the figure, the dot-dashed line denotes the peak value G_p of G

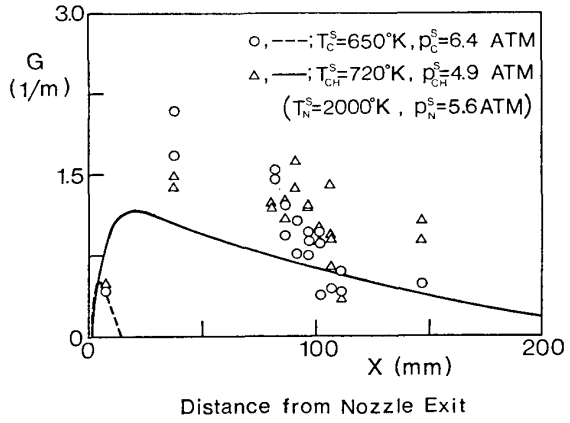

FIG. 20. Gain distribution along center of cavity from the exit of screen nozzle.

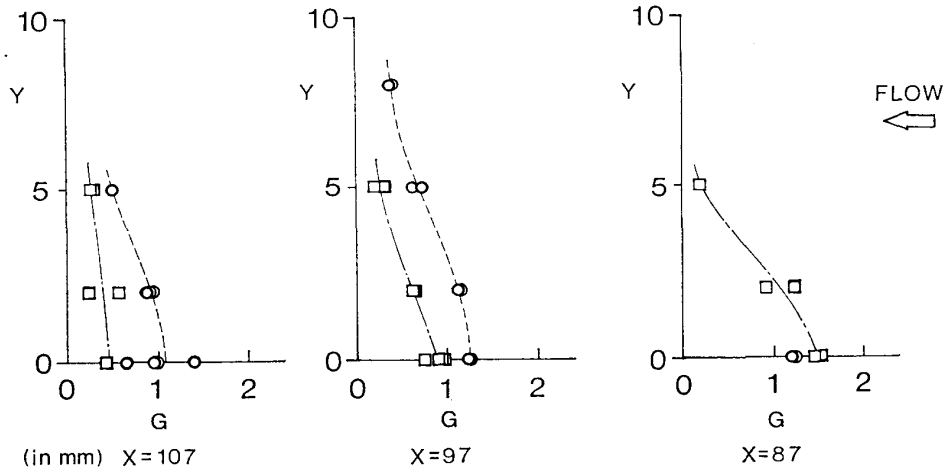

FIG. 21. Gain distributions normal to flow (for screen nozzle). ○: CO_2/He, □: pure CO_2

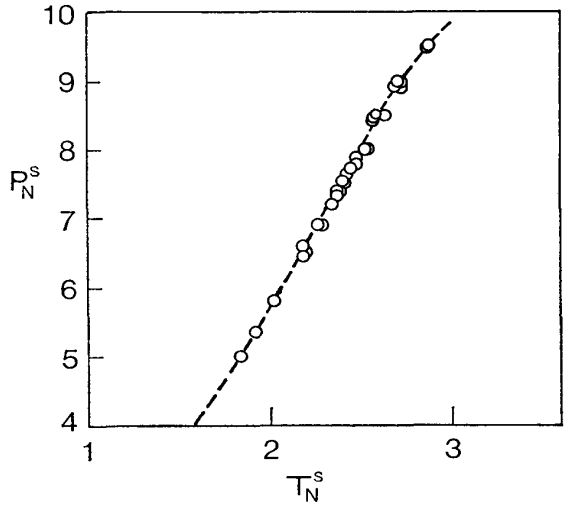

FIG. 22. Experimental stagnation conditions for N_2.

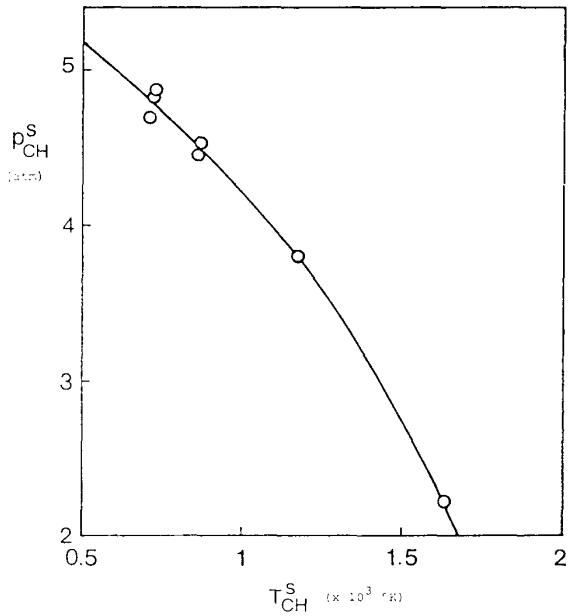

FIG. 23. Typical stagnation conditions of 50 CO_2/50 He for measurement.

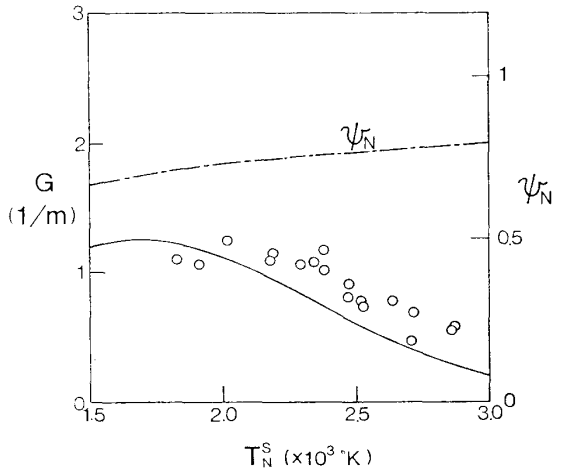

FIG. 24. Effect of N_2 stagnation condition on gain for fixed CO_2 stagnation; $T_{CH}{}^S$=720°K, $p_{CH}{}^S$=4.8 atm, CO_2: He=2:3, $A_C/A_C{}^*$=4.

appearing near the nozzle exit. As presumed, measured data lie lower than the estimate, and both results indicate qualitatively similar trend in the range of T_C^s below 1200°K. In the range of T_C^s above 1500°K, however, the experiment is scattered largely and show quite different distribution from the estimate. Unfortunately, we have no reasonable explanation on this discrepancy in the higher T_C^s. The effect of the addition of catalyst He on gain was not so distinct as in the estimate, so far as the present experiment is concerned.

Experimental results for a screen nozzle are compared with the estimate in the following. This nozzle consists of one row of six conical nozzles for CO_2 sandwiched by two rows of 8 conical nozzles for N_2, and faster CO_2/N_2 mixing is expected to

achieve than in 2-*D* nozzles. In Fig. 20 are shown both calculated and measured distributions of gain along the center line of the flow from the nozzle exit toward downstream. In our screen nozzle the area ratio of CO_2 nozzle is 1.8 with the throat of 3 mm in diam. (see Fig. 6). The equivalent molar fraction after mixing was $56N_2/44CO_2$ for the case without catalyst and $53N_2/19CO_2/28He$ for the case with catalyst. It can be seen from the figure that, in the case of mixture CO_2/He, qualitative behavior of measured gain distribution shows a trend similar to that from the estimate. The calculated gain, however, was lower than the experiment. This is likely to be mainly due to the fact that the measured gain on the axis takes the maximum in distribution along lines normal to axis, as shown in Fig. 21. The assumptions of the instantaneous mixing, neglection of viscous effect as well as wave disturbances must lead an over-estimate of *G*. Nevertheless, for the case of pure CO_2, the measured data indicate

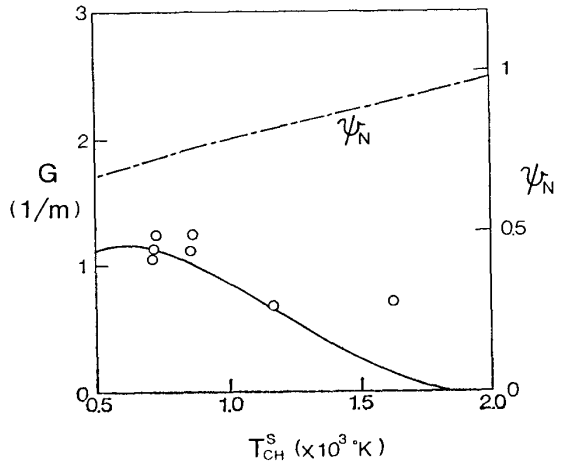

FIG. 25. Effect of CO_2 stagnation condition on gain for fixed N_2 stagnation; $T_N{}^S=2000°K$, $p_N{}^S=5.7$ atm, CO_2:He=2:3, $A_C/A_C{}^*=4$.

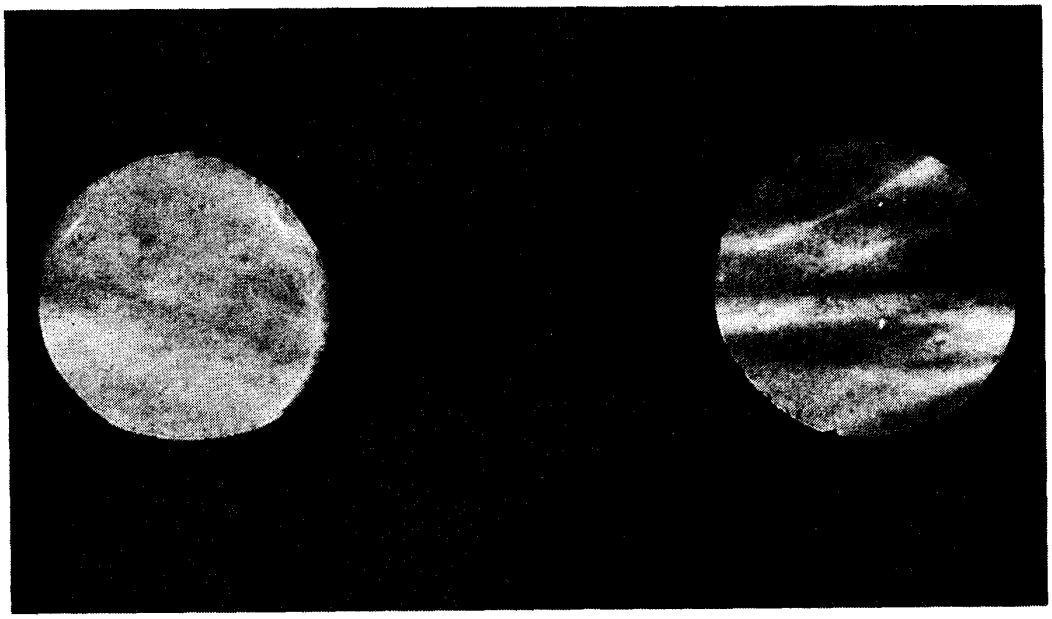

FIG. 26. Schlieren photograph of mixed flow in the vicinity of screen nozzle end.

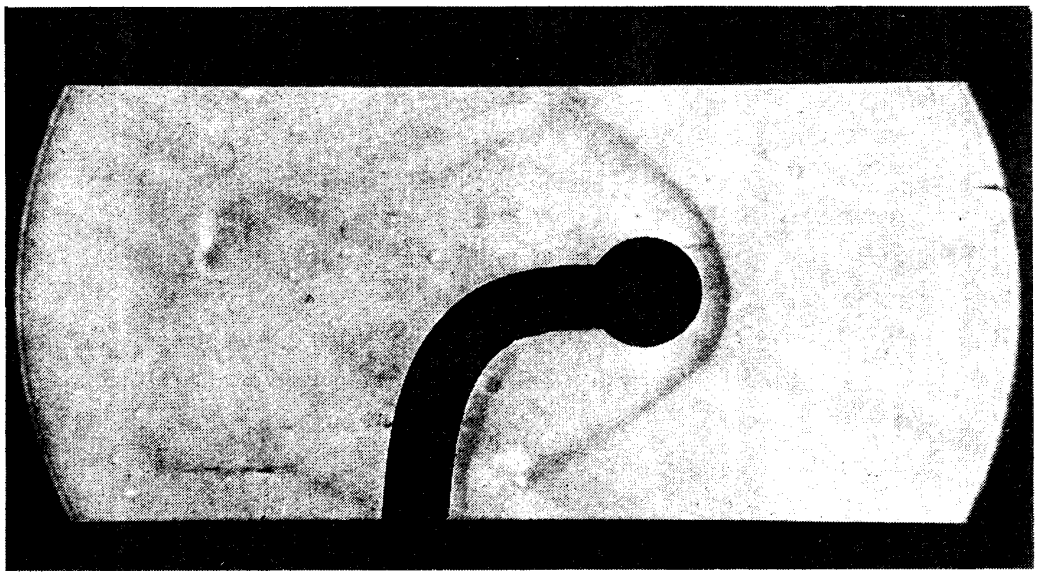

FIG. 27. Schlieren photograph of mixed flow in cavity (with obstacle).

much greater gain distribution than the estimate. Physical explanation must remain in future study. The catalyst He affects to make smaller decay rate of G after the maximum.

In order to clarify the dependence of G on the stagnation conditions, the gain at the cavity center was measured with varying N_2 stagnation conditions for a fixed condition of CO_2, and vice versa. These conditions are shown in Figs. 22 and 23. The results are demonstrated in Figs. 24 and 25, where the calculated gain is also plotted with full line, together with the equivalent molar fraction ψ_N of N_2. The estimated results indicate fairly good agreement with the experiment. It should be noted that there exists an optimum stagnation condition for N_2/CO_2 supersonic mixing GDL with a specified nozzle configuration. In the range of T^s_{CH} above 1500°K, the experimental data are likely to indicate a trend somewhat different from that of the estimate, as seen in the cases of 2-D nozzle.

Finally, the flow fields observed by Schlieren method are shown in Figs. 26 and 27. Figure 27 is taken for the flow around a cylinder inserted in the cavity. It can be seen that there is a smooth bow shock wave, not much disturbed.

CONCLUDING REMARKS

Experimental study on CO_2/N_2 mixing gasdynamic laser by the synchronized operation of two shock tubes is performed together with the numerical estimate based on the assumptions of instantaneous mixing, quasi-onedimensional inviscid flow, and three-mode model of vibrational relaxationin $CO_2/N_2/He$ system. The results can be summarized as follows:

1) Synchronization of two shock tubes is successfully achieved with the mismatch less than 400 μs by the electrical control of nondiaphragm driving mechanism with free piston.

2) For the mixing GDL using both two-dimensional and conical nozzles, the measured data of small signal gain coefficient are simulated qualitatively by the estimate except for higher CO_2 stagnation temperature range above 1500°K.
3) From the numerical comparison among several types of mixing schemes, the downstream mixing of N_2 with expanded CO_2 indicates most favorable characteristics of lasing performance. Furthermore, in the experiment the downstream mixing scheme by a screen nozzle indicates a favorable performance superior to that by the two-dimensional nozzle.
4) The existence of optimum stagnation conditions for both flows of CO_2 and N_2 is clarified experimentally and also analytically for a fixed nozzle configuration.
5) Besides the gain measurement, the measurement of lasing power and the observation of mixed flow field by Schlieren method are conducted supplementarily.

Acknowledgements

The authors are grateful to express their thanks to Prof. S. Tsuchiya, University of Tokyo for his great help for the arrangement of infrared detector and CW CO_2 laser, to Dr. W. Masuda of Ishikawajima-Harima Heavy Industry Co. Ltd. for his valuable discussion of the numerical computation, and also to Mr. K. Yonezu of Chiba University (at present Japan Patent Office) for his technical assistances.

Department of Aerodynamics and Structures
Institute of Space and Aeronautical Science
University of Tokyo
23 December 1980

References

[1] J. D. Anderson, Jr.: *Gasdynamic Lasers: An Introduction*, Academic Press, New York, 1976.
[2] R. I. Soloukhin: "Shock Tubes in Flow Laser Research; Modeling and Application," *Shock Tube and Shock Wave Research* (Proc. 11th Int. Symp. on Shock Tubes and Waves), University of Washington Press, 1978, pp. 629–644.
[3] P. E. Cassady, A. L. Pindroh, and J. F. Newton: "Performance Potential of Advanced GDL Concepts," *AIAA Journal*, Vol. 17, No. 8, 1979, pp. 845–853.
[4] J. P. E. Taran, M. Charpenel, and R. Borghi: "Investigation of a Mixing CO_2 GDL," *AIAA Paper*, No. 73–622, 1973.
[5] V. N. Croshko, N. A. Fomin, and R. I. Soloukhin: "Population Inversion and Gain Distribution in Supersonic Mixed Flow Systems," *Acta Astronautica*, Vol. 2, Pergamon Press, 1975, pp. 929–939.
[6] P. E. Cassady, J. Newton, and P. Rose: "A New Mixing Gasdynamic Laser," *AIAA Paper*, No. 76–343, 1976.
[7] W. Schall, P. Hoffmann, and H. Hügel: "Performance of N_2/CO_2 Gasdynamic Mixing Lasers with Various Injection Techniques," *Journal of Applied Physics*, Vol. 48, No. 2, 1977, pp. 688–690.
[8] P. E. Cassady: "A Survey of Advanced Gasdynamic Laser Concepts," *Gas-Flow and Chemical Lasers* (Proc. 2nd Int. Symp. on Gas-Flow and Chemical Lasers, Belgium), Hemisphere Publishing Corporation, 1979, pp. 95–127.

[9] R. Bailly, M. Pealat, and J. P. E. Taran: "Toward a Combustion-Driven Mixing GDL," *Revue de Physique Appliquee*, Vol. 12, 1977, pp. 1705–1710.

[10] V. N. Croshko, R. I. Soloukhin, and N. A. Fomin: "Effect of the Composition and Temperature of the Medium on the Efficiency of the Thermal Excitation of Inversion by Mixing in a Supersonic Flow," *Combustion, Explosion, and Shock Waves* (A Translation of *Fizika Goreniya i vzryva*), Vol. 10, No. 4, 1974, pp. 410–419.

[11] A. V. Krauklis, V. N. Croshko, R. I. Soloukhin, and N. A. Fomin: "Generating Conditions in a Gasdynamic Laser with Thermal Excitation and Mixing in a Supersonic Flow," *Combustiin, Explosion, and Shock Waves*, Vol. 12, No. 5, 1977, pp. 709–712.

[12] H. Oguchi, K. Funabiki, S. Sato, and K. Maeno: "An Experimental Study on CO_2 Gasdynamic Laser by Means of Non-Diaphragm Shock Tubes," *Bulletin of ISAS*, Univ. of Tokyo, Vol. 14, No. 2(B), 1978, pp. 809–829 (in Japanese).

[13] H. Oguchi, K. Funabiki, and S. Sato: "A New Type of the Shock Valve and its Characteristic Performance," *ISAS RN20*, Univ. of Tokyo, 1976.

[14] J. D. Anderson, Jr.: "Navier-Stokes Solutions of High Energy Laser Flows," *Gas-Flow and Chemical Lasers*, Hemisphere Publishing Corporation, 1979, pp. 3–21.

[15] N. G. Basov, V. G. Mikhailov, A. N. Oraevskii, and V. A. Shcheglov: "Molecular Population Inversion in the Supersonic Flow of a Binary Gas in a Laval Nozzle," *Soviet Physics—Technical Physics*, Vol. 13, No. 12, 1969, pp. 1630–1636.

[16] G. Lee: "Quasi-One-Dimensional Solution for the Power of CO_2 Gasdynamic Lasers," *The Physics of Fluids*, Vol. 17, No. 3, 1974, pp. 644–649.

[17] G. Kamimoto, H. Matsui, and K. T. Len: "A Study of CO_2 Gas-Dynamic Lasers; Part 1 Theoretical and Numerical Analysis," *Kyoto University Current Papers, CP-38*, 1973.

[18] Y. Sato and S. Tsuchiya: "Vibrational Relaxation Equation for Polyatomic Gases and Its Application to CO_2," *Journal of the Physical Society of Japan*, Vol. 30, No. 5, 1971, pp. 1467–1476.

[19] R. L. Taylor and S. Bitterman: "Survey of Vibrational Relaxation Data for Processes Important in the CO_2-N_2 Laser System," *Reviews of Modern Physics*, Vol. 41, No. 1, 1969, pp. 26–47.